The non-innocent role of graphene in the formation/immobilization of ultra-small gold nanoparticles functionalized with N-heterocyclic carbene ligands

David Ventura-Espinosa,[a] *Santiago Martín*[b,c] *and Jose A. Mata*[*a]

[a]Institute of Advanced Materials (INAM), Centro de Innovación en Química Avanzada (ORFEO-CINCA), Universitat Jaume I, Avda. Sos Baynat s/n, 12006, Castellón (Spain). Fax: (+34) 964387522; Tel.: (+34) 964387516; e-mail: jmata@uji.es

[b]Departamento de Química Física, Facultad de Ciencias, Universidad de Zaragoza, C/Pedro Cerbuna 12 50009 Zaragoza (Spain).

[c]Instituto de Ciencias de Materiales de Aragón (ICMA), C/Pedro Cerbuna 12, Universidad de Zaragoza-CSIC, 50009 Zaragoza (Spain).

Keywords: Gold nanoparticles, supported catalysis, graphene, hybrid materials, alkyne hydration

Abstract

Ultra-small gold nanoparticles (AuNPs) are obtained by treatment of well-defined gold complexes with reduced graphene oxide (rGO) without any auxiliary reducing agent. The AuNPs are functionalized with N-heterocyclic carbene (NHC) ligands, which allow controlling both the size and morphology, avoiding aggregation. The AuNPs are directly immobilized on the surface of graphene yielding hybrid materials composed of metal nanoparticles and a carbonaceous support. The catalytic properties of these AuNPs immobilized onto graphene have been tested in the hydration of alkynes. The AuNPs showed superior

catalytic activity vs. the parent molecular gold complexes and were recycled up to ten times. We have observed that graphene plays an important role in the stabilization of AuNPs functionalized with NHC ligands.

1. Introduction

Metal nanoparticles (MNPs) have attracted considerable attention in many research areas and particularly in the field of catalysis.[1–6] However, they suffer from the Oswald ripening phenomenon a common feature for metal nanoparticles (MNPs) employed in catalytic applications. To tackle this problem, different stabilizing agents such as surfactants, polymers or ligands have been used as coating agents.[7–12] Unfortunately, the presence of these coating agents may block the mass transport preventing direct contact between the reagents and the catalytic active sites. [13–18] Therefore, the design of efficient catalysts based on MNPs requires the use of labile coating agents in combination with supports to enhance stability.[19–24] In the last years, many efforts have been devoted to develop AuNPs functionalized with different types of ligands. However, examples dealing with the combination of the ligands with any supports are scarce.[25–34]

Graphene among others, has emerged as a promising support, since combines a high surface area with a strong interaction with MNPs enabling the preparation of catalytic hybrid materials, which display improved activity, selectivity and stability.[35–39] In this context, we recently described a direct approach for the immobilization of well-defined organometallic complexes onto the surface of graphene (Figure 1).[40–42] The forces that maintain the complexes onto the surface of graphene are π-stacking interactions between polyaromatic groups and the p cloud electron density of graphene. These non-covalent interactions are particularly strong when pyrene is used as a polyaromatic group. This methodology allows us to obtain a homogeneous distribution of well-defined complexes over the entire graphene surface and not only at the edges/defects or at the functional groups. The hybrid materials displayed interesting catalytic properties in the dehydrogenation of alcohols [43] and primary amines [44], in the coupling of silanes with alcohols [45,46] and in the intramolecular hydroamination of alkynes. [47] Interestingly, these hybrid materials show increased catalytic activity compared to the parent molecular complexes. This enhancement of catalytic properties is not common in the heterogeneization of molecular complexes suggesting that graphene plays an important role in the catalytic process. Additionally, these hybrid catalytic materials were recycled up to ten times without loss of activity. The properties of the organometallic complexes and the support are preserved during immobilization because of the mild conditions used in the procedure, which allows a rationale design of heterogenized molecular catalysts.

Herein we now report, a synthetic methodology for the preparation of a hybrid catalyst comprised of AuNPs functionalized with NHC ligands supported onto graphene (Figure 1). The hybrid catalyst is

obtained from the direct reaction of NHC-Au complexes and graphene without any reducing agent. Its preparation reveals the non-innocent role of graphene on the formation/immobilization of AuNPs. This new platform efficiently catalyze the hydration of alkynes [48–52] which is an environmentally friendly methodology for obtaining carbonyl derivatives by the addition of water. [53–57] In addition, the hybrid material shows high activity at low catalysts loadings, does not require additives and is highly recyclable.

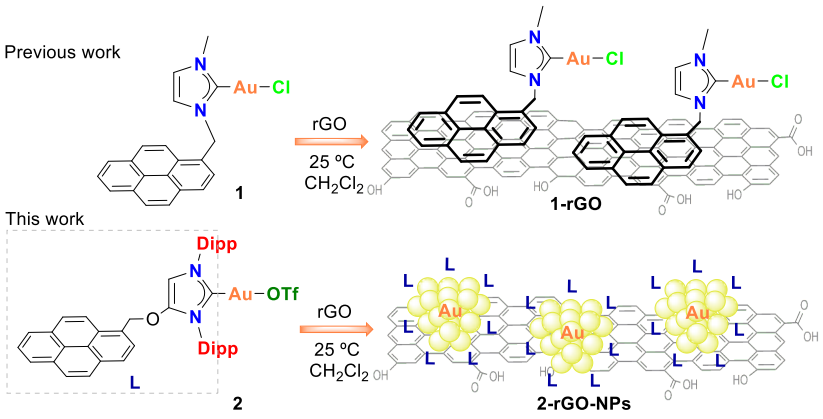

Figure 1. Synthesis of the hybrid material **1-rGO** containing a well-defined gold complex (**1**) immobilized onto graphene and synthesis of the hybrid catalyst **2-rGO-NPs** containing gold nanoparticles functionalized with NHC ligands (**L**). Dipp = 2,6-diisopropylphenyl.

2. Experimental Section

2.1. General procedures

Anhydrous solvents were dried using a solvent purification system. 4-hydroxy-1,3-(2,6-diisopropylphenyl)imidazolium chloride [58] and bromomethyl pyrene [59] were prepared according to reported procedures. Nuclear magnetic resonance (NMR) spectra were recorded on Bruker spectrometers operating at 300 or 400 MHz (^{1}H NMR) and 75 or 100 MHz (^{13}C{^{1}H} NMR), respectively, and referenced to $SiMe_4$ (δ in ppm and J in Hertz). NMR spectra were recorded at room temperature with the appropriate deuterated solvent. Elemental analysis were carried out in a TruSpec Micro Series. Electrospray Mass Spectra (ESI-MS) were recorded on a MicroMass Quatro LC instrument. MeOH was used as mobile phase and nitrogen was used as the drying and nebulizing gas. Scanning electron microscopy images (SEM), were taken with a field emission gun scanning electron microscope model JEOL 7001F. High-resolution images of transmission electron microscopy (HRTEM) and high-angle annular dark-field (HAADF-STEM) images of the samples were obtained using a Jem-2100 LaB6 (JEOL) transmission electron

microscope coupled with an INCA Energy TEM 200 (Oxford) energy dispersive X-Ray spectrometer (EDX) operating at 200 kV. Samples were prepared by drying a droplet of a MeOH dispersion on a carbon-coated copper grid. X-ray photoelectron spectra (XPS) were acquired on a Kratos AXIS ultra DLD spectrometer with a monochromatic Al Kα X-ray source (1486.6 eV) using a pass energy of 20 eV. To provide a precise energy calibration, the XPS binding energies were referenced to the C1s peak at 284.6 eV. GC analyses were obtained on a shimadzu GC-2010 apparatus equipped with a FID detector, and using a Teknokroma column (TRB-5MS, 30 m x 0.25 mm x 0,25 μm). UV-vis spectra were acquired on a Varian Cary 50 spectrophotometer.

2.2. General procedure for the hydration of alkynes

In a Pyrex® tube and under air, the corresponding alkyne (1 eq.) water (2 eq.), catalyst (**2 or 2-rGO**), and Methanol (concentration of alkyne 0.15 M) were mixed. The reaction was stirred at 50 ºC in an oil bath. Conversion of alkyne into the corresponding ketone was monitored by GC-FID using anisole as an internal standard. When the reaction was completed the solvent was removed and the yield of the isolated product analyzed by NMR.

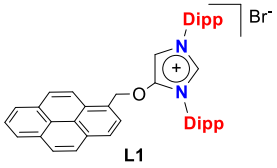

L1

2.3. Synthesis of the imidazolium salt L1

4-hydroxy-1,3-(2,6-diisopropylphenyl)imidazolium chloride (600 mg, 1.36 mmol) was suspended in 30 mL of dry acetonitrile. Potassium carbonate (234 mg, 1.7 mmol) and potassium bromide (490 mg, 4.08 mmol) were added and the mixture stirred at 0 ^{0}C for 1 h. Then, bromomethyl pyrene (482 mg, 1,63 mmol) was added and the mixture stirred for 2 h. at room temperature and heated at 60 ºC for 15 h. The solvent was removed and the residue was suspended in dichloromethane and was filtered to remove insoluble inorganic salts. Recrystallization from dichloromethane/ether at -18 ^{0}C afforded **L1** as a pale yellow powder. Yield: 410 mg (43 %). ^{1}H NMR (300 MHz, MeOD) δ 9.53 (d, J = 1.8 Hz, 1H, NC*H*N), 8.46 – 8.02 (m, 9H, CH_{pyr}), 7.97 (d, J = 1.8 Hz, 1H, CH_{imid}), 7.64 (m, 1H, CH_{arom}), 7.49 (m, 3H, CH_{arom}), 7.32 (m, 2H, CH_{arom}), 6.09 (s, 2H, CH_2), 2.72 – 2.44 (m, 2H, CH_{iPr}), 2.43 – 2.18 (m, 2H, CH_{iPr}), 1.32 (d, J = 6.8 Hz, 6H, C$H_{3,\ iPr}$), 1.21 (d, J = 6.9 Hz, 6H, C$H_{3,\ iPr}$), 1.10 (d, J = 6.9 Hz, 6H, C$H_{3,\ iPr}$), 0.95 (d, J = 6.8 Hz, 6H, C$H_{3,\ iPr}$). ^{13}C NMR (75 MHz, MeOD) δ [149.35, 147.08, 146.67, 135.09, 134.13] (C_{pyr}, $C_{,arom}$), , 133.36 (N*C*HN), [132.55, 132.08, 131.96, 131.30, 129.95, 129.70, 129.60, 128.26, 127.76, 127.63, 127.56, 127.19, 127.00, 126.10, 125.97, 125.80, 125.53, 123.59] (C_{pyr}, $C_{,arom}$, C_{imid}), 105.42 (*C*H$_{imid}$),

74.93 (CH_2) , [30.51, 30.33] (CH_{iPr}) , [24.89, 24.71, 24.05, 23.15] ($CH_{3,\ iPr}$). Electrospray MS (Cone 20 V) (m/z, fragment): 619.4 $[M]^+$. Elemental Anal. Calculated for $C_{44}H_{47}N_2OBr$: C, 75.52; H, 6.77; N, 4.00 Found: C, 75.38; H, 6.74; N, 3.85.

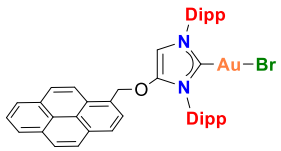

i1

2.4. Synthesis of complex i1

In a Pyrex® tube, imidazolium salt (**L1**) (218 mg, 0.31 mmol), [AuCl(SMe_2)] (91.8 mg, 0.31 mmol), K_2CO_3 (64.3 mg, 0.465 mmol) and 2 mL of acetone were heated at 60 ^{0}C for 18 h. Then, the solvent was removed under vacuum, dichloromethane was added (10 mL) and the mixture was filtered through silica. The pad of silica was washed with dichloromethane (10 mL). The solvent was reduced to ca. 2 mL and pentane was added, affording an orange solid, which was filtered and dried under vacuum. Yield: 185 mg (66%). ^{1}H NMR (300 MHz, $CDCl_3$) δ 8.23 (d, J = 7.9 Hz, 2H, CH_{pyr}), 8.15 – 7.99 (m, 6H, CH_{pyr}), 7.90 (d, J = 7.9 Hz, 1H, CH_{pyr}), 7.54 – 7.38 (m, 2H, CH_{arom}), 7.27 – 7.13 (m, 4H, CH_{arom}), 6.42 (s, 1H, CH_{imid}), 5.74 (s, 2H, CH_2), 2.62 (m, 4H, CH_{iPr}) 1.33 (dd, 12H, C$H_{3,\ iPr}$), 1.19 (d, J = 6.9 Hz, 6H, C$H_{3,\ iPr}$), 1.12 (d, J = 6.9 Hz, 6H, C$H_{3,\ iPr}$). ^{13}C NMR (75 MHz, $CDCl_3$) δ 173.67 ($C_{carbene}$-Au), 147.89 (C_{imid}), [146.16, 145.72] (C_{arom}), [134.62, 132.26, 131.16, 130.78, 130.56, 130.31, 129.42, 128.73, 128.41, 127.19, 126.78, 126.59, 126.40, 126.02, 125.84, 124.87, 124.48, 124.18, 124.12, 122.10] (C_{Pyr}, C_{arom}), 100.95 (CH_{imid}), 73.12 (CH_2), [29.13, 28.73] (CH_{iPr}), [24.64, 24.43, 24.08, 23.61] ($CH_{3,\ iPr}$). Electrospray MS (Cone 20 V) (m/z, fragment): 935.0 $[M+K]^+$. Elemental Anal. Calculated for $C_{44}H_{46}N_2OAuBr$: C, 59.00; H, 5.18; N, 3.13 Found: C, 59.3; H, 5.42; N, 3.09.

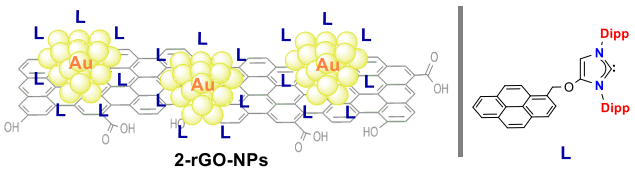

2-rGO-NPs L

2.5. Synthesis of **2-rGO-NPs**

A suspension of 490 mg of rGO in 350 mL of CH_2Cl_2 in a round bottom flask was immersed in an ultrasounds bath for 30 min. In a Schlenk flask and under the protection of light, complex **i1** (150 mg, 0.166 mmol) and Silver triflate (56.4mg, 0.184 mmol) were dissolved in 8 mL of dry CH_2Cl_2 and the mixture was stirred at room temperature for 15 min. Then the reaction was filtered through a long pad of

Celite®. The solvent was reduced in the rotatory evaporator until ca. 5 mL. Then, this mixture was added to the suspension of rGO in CH_2Cl_2 and was stirred at room temperature for 48 h. The black solid was isolated by filtration and washed with 200 mL of CH_2Cl_2 affording the hybrid material **2-rGO-NPs**. The exact amount of supported complex was determined by ICP-MS analysis. The results accounted for a 0.018 mg Au/100 mg rGO of gold in the hybrid material **2-rGO-NPs.** The hybrid material was characterized by SEM, HRTEM, UV-Vis and XPS (See details in SI). An aliquot of the in situ formed complex **2** was dried and analyzed by ^{1}H NMR and ESI/MS. ^{1}H NMR (300 MHz, $CDCl_3$) δ 8.23 (d, *J* = 7.7 Hz, 2H, C*H*$_{pyr}$), 8.16 – 8.00 (m, 6H, C*H*$_{pyr}$), 7.91 (d, *J* = 7.8 Hz, 1H, C*H*$_{pyr}$), 7.47 (m, 2H, C*H*$_{arom}$), 7.25 (m, *4*H, C*H*$_{arom}$), 6.51 (s, 1H, C*H*$_{imid}$), 5.76 (s, 2H, C*H*$_2$), 2.68 – 2.30 (m, 4H, C*H*$_{iPr}$), 1.40 – 1.03 (m, 24H, C*H*$_3$, $_{iPr}$). Electrospray MS (Cone 20 V) (m/z, fragment): 847.3 [M-OTf $^-$+MeOH]$^+$.

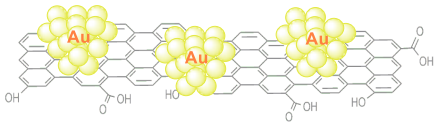

$HAuCl_4$-rGO-NPs

2.6. Synthesis of **$HAuCl_4$-rGO-NPs**

A suspension of rGO (90 mg) in CH_2Cl_2 (65 mL) was immersed in an ultrasounds bath for 30 min. Then, $HAuCl_4 \cdot 3H_2O$ (22.5 mg, 0.06 mmol) was added to the suspension and was stirred at room temperature for 48 h. The black solid was isolated by filtration and washed with 100 mL of CH_2Cl_2 affording the hybrid material **$HAuCl_4$-rGO-NPs**. The exact amount of supported complex was determined by ICP-MS analysis. The results accounted for a 0.028 mg Au/100 mg rGO of gold in the hybrid material **$HAuCl_4$-rGO-NPs.**

3. Results and Discussion

3.1. Synthesis and characterisation

We have previously immobilized the gold complex **1** onto reduced graphene oxide (rGO) generating the hybrid material **1-rGO** (Figure 1). [47] The procedure consisted in the exfoliation of rGO by ultrasounds (30 min) and stirring in the presence of the molecular gold complex (10 h). Microscopy analysis by HRTEM revealed the homogeneous distribution of gold and the absence of metal nanoparticles. A comparative high-resolution XPS analysis of **1** and **1-rGO** showed that the core-level peaks of gold, nitrogen and chloride appear at the same binding energies, indicating the presence of the molecular complex onto the graphene surface. Considering these results, we sought to immobilize complex **2** on the

surface of reduced graphene oxide using the same methodology (Scheme 1). Synthesis of **2** is carried out by a two-step process starting from the imidazolium salt **L1**. This imidazolium salt contains the pyrene-tag at the backbone of the azol ring instead of at the nitrogen. This allows the design of NHC ligands containing bulky protecting groups such as the 2,6-diisopropylphenyl (Dipp). The metalation of **L1** under basic conditions produces the Au(I) intermediate complex **i1** that has been completely characterized including the single X-ray crystal structure (See SI for details). Treatment of **i1** with a silver salt allows the introduction of a labile OTf^- ligand that is very convenient in the design of homogeneous catalysts.[55] The immobilization of complex **2** on the surface of graphene gave results completely different to complex **1**. The gold complex **2** is stable in the solid state and in solution but decomposes in the presence of rGO forming gold nanoparticles (**2-rGO-NPs**) that are directly immobilized on the surface of graphene. These AuNPs are produced under mild reaction conditions which prevent side reactions and alteration of the support. The AuNPs on the surface of graphene are characterized by transmission microscopy (HRTEM), X-ray photoelectron spectroscopy (XPS) and UV/vis spectroscopy. HRTEM analysis confirms the presence of ultrasmall and spherical shape AuNPs (Figure 2a-b). The particle size histogram reveals a distribution with an average diameter of 3.2 ± 1.5 nm (n = 450) (Figure 2c). We have not observed an increase in the size of AuNPs for prolonged reaction times indicating that graphene controls the growing of NPs. Thus, reduced graphene oxide acts as a stabilizer controlling the size and shape of these AuNPs. We have previously evidenced that graphene stabilizes PdNPs and also that control the size and morphology.[60] XPS analysis confirms the presence of NHC ligands and anions (OTf^-) at the surface of the AuNPs by the assignment of the core-level peaks of N (400.7 eV) and F (688.0 eV). The Au 4f region of **2-rGO-NPs** shows a doublet peak ($4f_{7/2}$ and $4f_{5/2}$) at a binding energy of 88.8 and 85.1 eV, suggesting the presence of Au(I) at the surface of the AuNPs (Figure 2d). These results are in agreement with the formation of AuNPs functionalized with chiral NHC ligands recently reported by Toste and Somorjai, where XPS analysis and XANES confirm the presence of a Au(I) monolayer at the surface of the nanoparticle [61]. The UV/vis spectroscopy shows the characteristic surface plasmon resonance of gold nanoparticles at 510 nm (Figure S4).

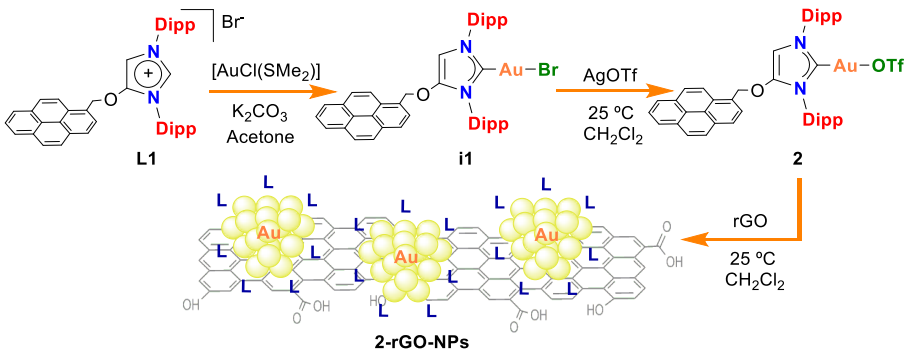

Scheme 1. Synthesis and immobilization of AuNPs on the surface of graphene.

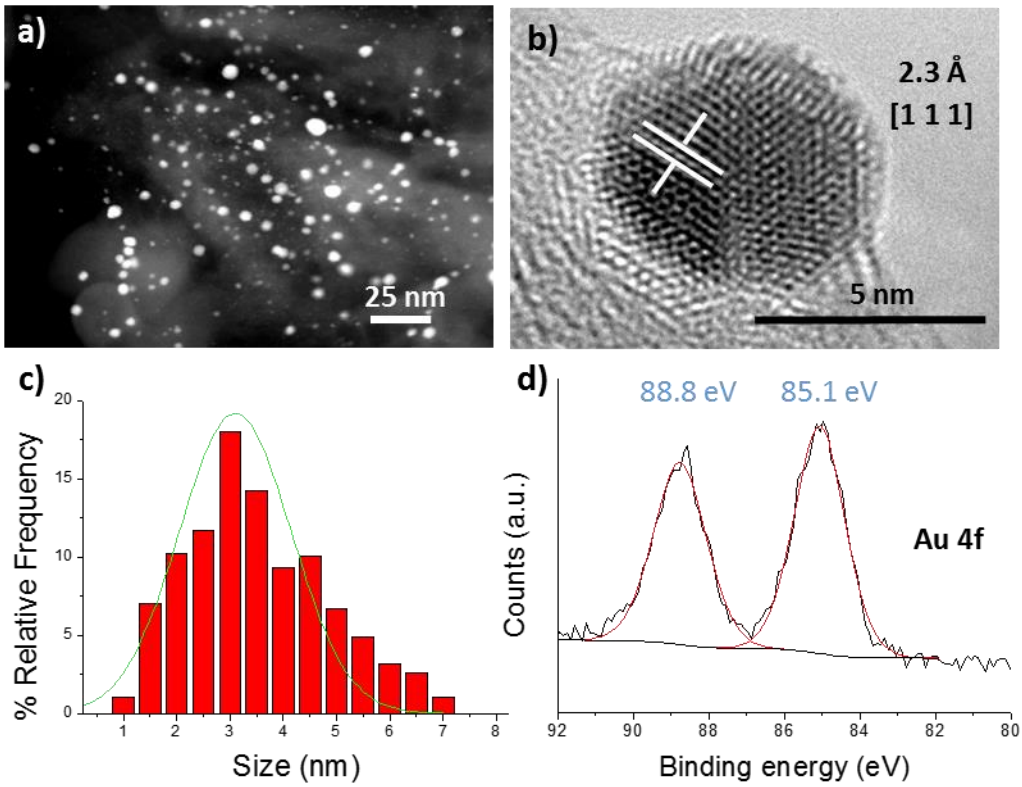

Figure 2. Characterization of gold nanoparticles onto graphene (**2-rGO-NPs**): a) Dark field TEM micrograph showing spherical AuNPs onto graphene. b) HRTEM micrograph showing the interplanar spacing. c) Size distribution histogram of the AuNPs (n = 450) and d) XPS analysis of the core-level peaks (eV) for the Au 4f region of **2-rGO-NPs**.

Based on these precedents, we decided to investigate the synthesis of AuNPs anchored onto graphene in order to get a better insight of the formation procedure. The synthesis of AuNPs functionalized with NHC ligands anchored on rGO is general and works under different reaction conditions. For instance, using methanol or ethanol yields similar AuNPs/rGO hybrid materials. For comparative purposes and in order to evaluate the ligand effect in the design of nanoparticles, we synthesized AuNPs lacking of NHC ligands using the commercially available $HAuCl_4$. Addition of a solution of $HAuCl_4$ to an exfoliated suspension of rGO leads to the formation of AuNPs immobilized on the surface of graphene (**$HAuCl_4$-rGO-NPs**). Characterization by HRTEM confirms the formation of larger AuNPs compared to **2-rGO-NPs**. The histogram shows a wide particle size distribution with an average diameter of 12.4 ± 4.2 nm (n = 74) (Figure 3). The AuNPs synthesised from $HAuCl_4$ lacking of NHC ligands (**$HAuCl_4$-rGO-NPs**) showed an increased average size of 9.2 nm vs. **2-rGO-NPs**, indicating that the presence of NHC ligands has an

important impact in the size of the nanoparticle. The combination of gold complexes containing NHC ligands with graphene is a convenient procedure for the synthesis of hybrid catalytic materials containing ultrasmall AuNPs.

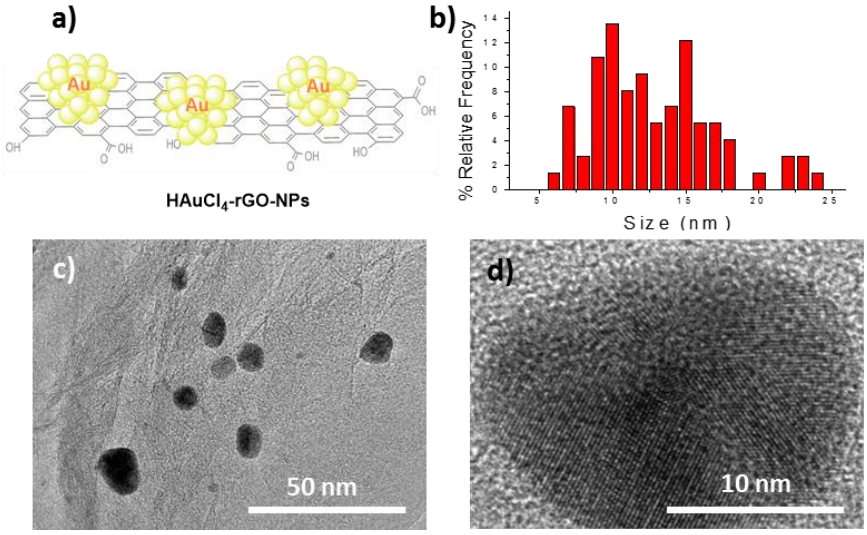

Figure 3. Characterization of AuNPs without capping ligands. a) Model for **HAuCl$_4$-rGO-NPs**. b) Size distribution histogram of AuNPs (n = 74). c) HRTEM micrograph showing spherical AuNPs onto graphene. d) HRTEM micrograph showing the interplanar spacing.

3.2. Catalytic properties

The catalytic performance of gold complexes and gold nanoparticles were evaluated in the hydration of alkynes. Optimization of the reaction conditions was made using 4-octyne as model substrate (SI, S11). The results showed that the additives (AgOTf) and the support (rGO) are not catalytic active species in the hydration of alkynes. The gold complex **i1** was completely inactive and the $HAuCl_4$ displayed modest conversion (18%) implying a limited catalytic activity. The best catalysts in the hydration of 4-octyne were the gold complex **2** and the AuNPs **2-rGO-NPs**. Full conversions were obtained in short reaction times and low catalyst loadings. Interestingly the gold nanoparticles without capping ligands (**HAuCl$_4$-rGO-NPs**) were completely inactive in the hydration of 4-octyne. Most probably the lack of catalytic activity is due to a large particle size distribution and the absence of stabilizing NHC ligands. Catalysts **2** and **2-rGO-NPs** were both competent in the hydration of a variety of alkynes suggesting a wide reaction scope (Figure 4a). We made a comparison of the catalytic activity of the best catalytic systems (**2** and **2-rGO-NPs**) for different substrates (SI, S11). The experimental results indicate that, while catalyst **2-rGO-NPs** is active even at very low catalyst loadings (0.02 mol%), the molecular complex **2**, requires a tenfold

higher catalyst loading to reach similar outcomes. As an example, the reaction monitoring profile in the hydration of 4-octyne afforded quantitative yield after 60 min using a catalyst **2-rGO-NPs** (0.02 mol%) but required 150 min in the case of catalyst **2** using a loading of 0.25 mol% (Figure 4b). This observation is general and better catalytic outcomes were observed using catalyst **2-rGO-NPs** for a variety of substrates. In parallel, poisoning experiments were used to determine the nature of the active catalytic species derived from catalyst **2**. The hydration reaction of phenyl acetylene was carried out in the presence of poly(4-vinylpyridine) as a scavenger of gold molecular complexes and the Hg drop test was used as a scavenger of AuNPs (SI, S11.2). [62–65] The presence of Hg has no effect in the reaction but it is inhibited by the addition of poly(4-vinylpyridine). These experiments suggest that the catalytic active species derived from **2** is molecular in nature. In the case of catalysts **2-rGO-NPs**, we performed a Maitlis hot filtration test using the hydration of 4-octyne (SI, S11.3). After 10 min (GC conversion 38%), half of the reaction mixture was filtered off through celite at 50 ºC. The filtrate was maintained for 300 min under identical conditions, but the GC analysis indicated that no further hydration occurred (GC conversion 53%, TOF = 240 h^{-1}). On the contrary, the remaining mixture achieved full conversion in less than 50 min (TOF = 4360 h^{-1}). Analysis of the apparent reaction rates and TOF values of the filtrate and the solid catalyst confirms the heterogeneous nature of **2-rGO-NPs** and suggests that the AuNPs are strongly attached to the support. The direct synthesis and immobilization of AuNPs onto graphene lead to a more efficient catalytic system in terms of activity and catalysts loading.

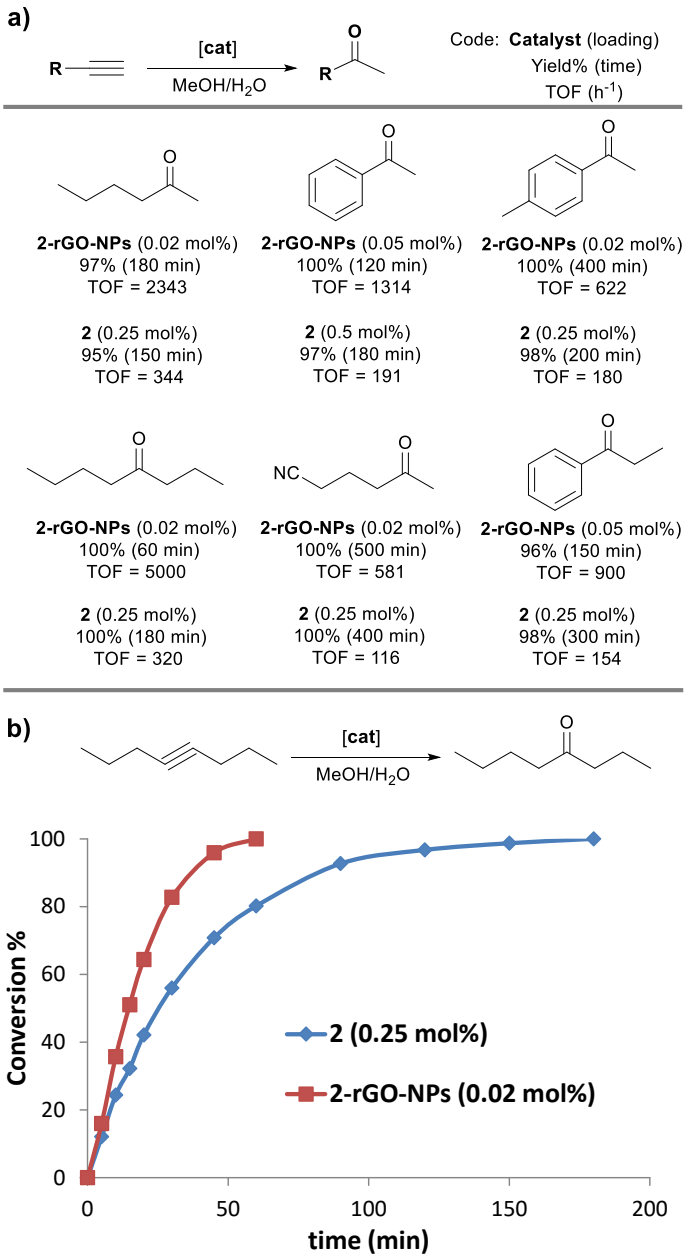

Figure 4. Summary of the catalytic properties of **2** and **2-rGO-NPs** in the hydration of alkynes. Conversions determined by GC/FID and yields calculated by ^{1}H NMR using 1,3,5-trimethoxybenzene as an internal standard. TOF values calculated at 1 h reaction. a) Reaction scope. b) Reaction profile of **2** vs **2-rGO-NPs** in the hydration of 4-octyne using MeOH as solvent, H_2O (2 eq.) at 50 ºC.

3.3. Recycling studies

The stability and recycling properties of the hybrid catalytic material **2-rGO-NPs** were evaluated in the hydration of alkynes using 4-octyne as model substrate. In a typical run were added 4-octyne, MeOH, H_2O (2 Eq.) and catalyst **2-rGO-NPs** (0.05 mol %) and the mixture was heated at 50 °C for the appropriate time. The reaction progress was monitored by GC until full conversion. After each run, the catalyst **2-rGO-NPs** was removed from the solution by decantation washed with methanol, dried with pentane and reused. The hybrid material **2-rGO-NPs** was reused up to 5 times without a significant decrease in activity observing similar apparent rate constants in the reaction time profile (Figure 5a). Then, there is a gradual decrease in activity but quantitative yields are obtained in less than 200 min (runs 6 to 8). After run 8, the apparent rate constants decrease gradually. However, still quantitative yields are achieved in less than 400 min. In order to elucidate this deactivation process, we performed an analysis by HRTEM microscopy and XPS at the end of the recycling experiment and analyzed the gold amount by ICP/MS. The HRTEM images before and after the recycling experiments show similar properties for the morphology of reduced graphene oxide, indicating that the support is not altered during extended operation. A high magnification HRTEM micrograph confirms the crystallinity of AuNPs after the 10^{th} catalytic run (Figure 5c). More interesting is that the size and morphology of AuNPs supported on the surface of graphene remain almost intact after ten catalytic runs (Figure 5). Additionally, the XPS spectrum of the Au4f region at the end of the recycling experiment shows the same doublet peak at 88.6 and 84.9 eV to these observed for the hybrid catalytic material **2-rGO-NPs** before being used (Figure 5e). To rationalize a possible deactivation mechanism caused by leaching the amount of gold was analyzed by ICP/MS in the filtrate of each run and in the hybrid catalyst after the 10^{th} run. The gold amount in the filtrates corresponding to runs 1 to 5 revealed insignificant gold content. In the following runs, there is a gradual increase of gold content that correlates well with the decrease in catalytic activity. This result was confirmed by analyzing the gold amount of the hybrid catalyst after the recycling experiment. After digestion of the solid, ICP/MS analysis revealed that 50 wt % of the initial gold content is lost by leaching. This study supports that (1) the Ostwald ripening is negligible, (2) there is a strong interaction between the AuNPs and the surface of rGO (3) the rGO favors the stabilization of nanoparticles and (4) deactivation mechanism is caused by leaching of AuNPs. These results point out that **2-rGO-NPs** is a robust and recyclable catalytic hybrid material.

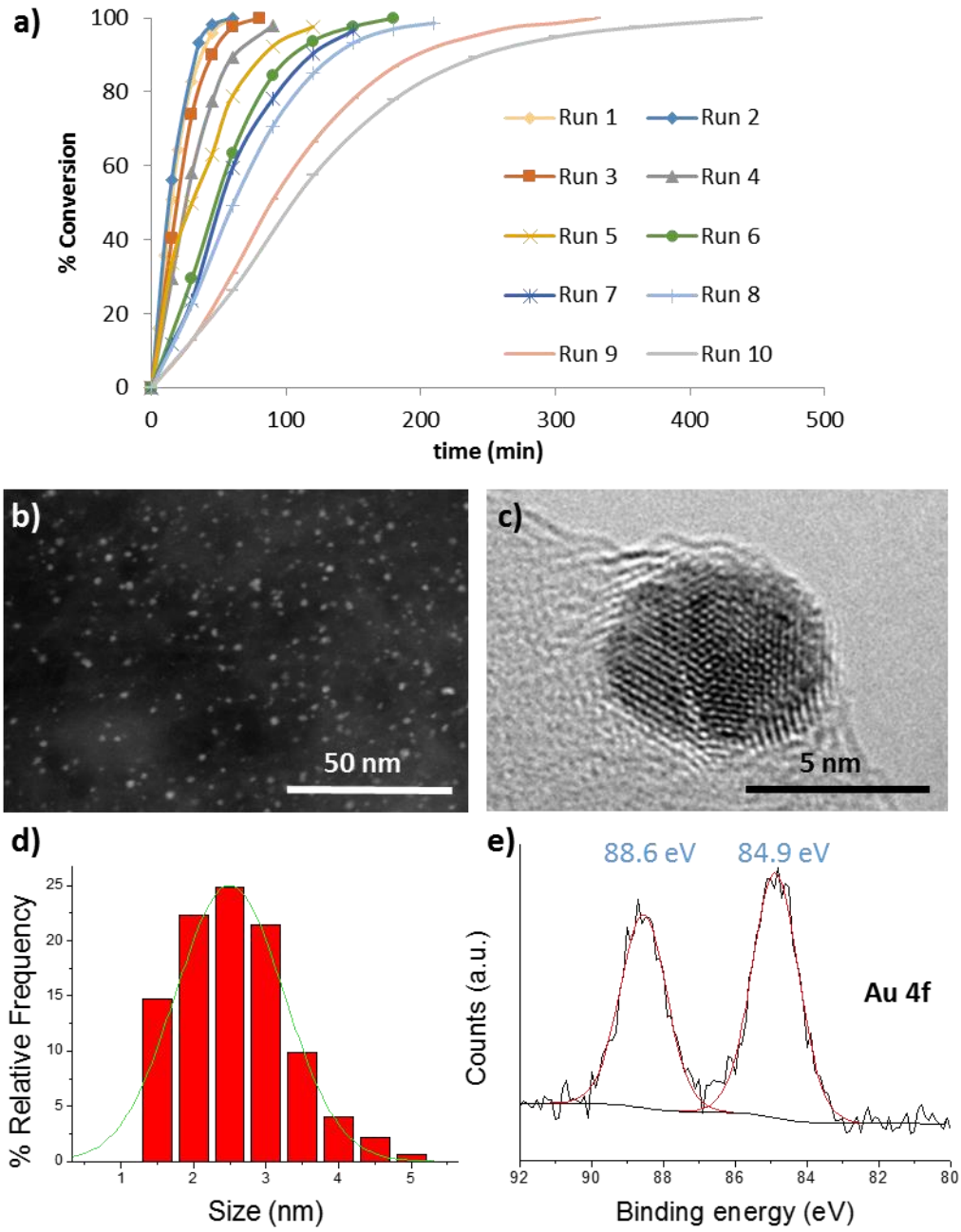

Figure 5. Recycling properties of **2-rGO-NPs** and catalyst characterization after the 10th run in the hydration of 4-octyne. a) Reaction profile of **2-rGO-NPs** for 10 consecutive runs in the hydration of 4-octyne using a catalyst loading of 0.05 mol% based on Au, MeOH/H_2O at 50 ºC. b) Dark field TEM micrograph showing spherical AuNPs onto graphene after the 10th run. c) High magnification HRTEM micrograph showing the crystallinity of an AuNP after the 10th run. d) Size distribution histogram after the 10th run (n = 292) and e) XPS analysis of the core-level peaks (eV) for the Au4f region after the 10th run.

4. Conclusions

Decomposition of a well-defined gold complex leads to AuNPs functionalized with NHC ligands anchored onto the surface of graphene. The AuNPs are produced under mild reaction conditions without any external reducing agent, highlighting the non-innocent role of graphene. The hybrid material composed of AuNPs and graphene as support is an efficient catalyst for hydration of alkynes. Interestingly, the AuNPs immobilized onto graphene show superior catalytic activity vs. the parent molecular complexes in terms of activity and stability. The catalytic system is recycled up to five times without significant degradation. Then, there is a gradual decrease in activity but quantitative yields are still obtained if the reaction time is increased. Studies by ICP/MS show that the deactivation mechanism is governed by gradual leaching of active species. Microscopy analysis after the catalytic experiments reveals that AuNPs maintain their integrity in terms of size and morphology. These experiments suggest that graphene plays an important role in the stabilization of AuNPs during catalysis. The presence of NHC ligands covering the AuNPs in combination with graphene represents a convenient approach to develop practical hybrid materials with catalytic properties. Future work will focus on a detail analysis of the interaction between the AuNPs and the support and its impact on catalytic activity.

Supporting information

Experimental details, complete characterization of metal complexes and hybrid materials, crystallographic data and reaction monitoring profiles. CCDC 1897736 contains the supplementary crystallographic data for this paper. These data can be obtained free of charge via www.ccdc.cam.ac.uk/data_request/cif, or by emailing data_request@ccdc.cam.ac.uk, or by contacting The Cambridge Crystallographic Data Centre, 12 Union Road, Cambridge CB21EZ, UK; fax: +44 1223 336033.

AUTHOR INFORMATION

Corresponding Author

*E-mail: jmata@uji.es. Fax: (+34) 964387522; Tel.: (+34) 964387516

ORCID

Jose A. Mata: 0000-0001-9310-2783

Santiago Martin: 0000-0001-9193-3874

David Ventura-Espinosa: 0000-0002-8777-5508

Author Contributions

The manuscript was written through contributions of all authors. All authors have given approval to the final version of the manuscript.

Funding Sources

MINECO (RTI2018-098237-B-C22) and (FPU15/03011), Universitat Jaume I (UJI-B2018-23) and DGA/fondos FEDER (E31_17R)

Notes

The authors declare no competing financial interest.

ACKNOWLEDGMENTS

The authors thank the financial support from MINECO (RTI2018-098237-B-C22) and Universitat Jaume I (UJI-B2018-23). D. V-E thanks the MINECO for a grant (FPU15/03011). S.M. acknowledges DGA/fondos FEDER (construyendo Europa desde Aragón) for funding the research group Platón (E31_17R). The authors are very grateful to the 'Servei Central d'Instrumentació Científica (SCIC)' of the Universitat Jaume I and Dr. G. Antorrena for the technical support in XPS studies.

REFERENCES

[1] J. Oliver-Meseguer, J.R. Cabrero-Antonino, I. Dominguez, A. Leyva-Perez, A. Corma, Science 338 (2012) 1452–1455.

[2] A. Primo, A. Corma, H. García, Phys. Chem. Chem. Phys. 13 (2011) 886–910.

[3] A. Corma, H. Garcia, Chem. Soc. Rev. 37 (2008) 2096–2126.

[4] M.-C. Daniel, D. Astruc, Chem. Rev. 104 (2004) 293–346.

[5] M. Boronat, A. Corma, J. Catal. 284 (2011) 138–147.

[6] M. Dhiman, B. Chalke, V. Polshettiwar, J. Mater. Chem. A 5 (2017) 1935–1940.

[7] C.M. Crudden, D.P. Allen, Coord. Chem. Rev. 248 (2004) 2247–2273.

[8] M.R. Narouz, C.-H. Li, A. Nazemi, C.M. Crudden, Langmuir 33 (2017) 14211–14219.

[9] L.D. Pachón, G. Rothenberg, Appl. Organomet. Chem. 22 (2008) 288–299.

[10] C. Richter, K. Schaepe, F. Glorius, B.J. Ravoo, Chem. Commun. 50 (2014) 3204–3207.

[11] M.J. MacLeod, J.A. Johnson, J. Am. Chem. Soc. 137 (2015) 7974–7977.

[12] M.-L. Wang, T.-T. Jiang, Y. Lu, H.-J. Liu, Y. Chen, J. Mater. Chem. A 1 (2013) 5923–5933.

[13] A. Ferry, K. Schaepe, P. Tegeder, C. Richter, K.M. Chepiga, B.J. Ravoo, F. Glorius, ACS Catal.

5 (2015) 5414–5420.

[14] P. Lara, O. Rivada-Wheelaghan, S. Conejero, R. Poteau, K. Philippot, B. Chaudret, Angew. Chem. Int. Ed. 50 (2011) 12080–12084.

[15] J.M. Asensio, S. Tricard, Y. Coppel, R. Andrés, B. Chaudret, E. de Jesús, Chem. Eur. J. 23 (2017) 13435–13444.

[16] L.C. Moraes, B. Lacroix, R.C. Figueiredo, P. Lara, J. Rojo, S. Conejero, Dalton Trans. 46 (2017) 8367–8371.

[17] Y. Segura, N. López, J. Pérez-Ramírez, J. Catal. 247 (2007) 383–386.

[18] K. Sharma nee Kamaldeep, S. Kaur, V. Bhalla, M. Kumar, A. Gupta, J. Mater. Chem. A 2 (2014) 8369–8375.

[19] C. Copéret, A. Comas-Vives, M.P. Conley, D.P. Estes, A. Fedorov, V. Mougel, H. Nagae, F. Núñez-Zarur, P.A. Zhizhko, Chem. Rev. 116 (2016) 323–421.

[20] M.K. Samantaray, J. Alauzun, D. Gajan, S. Kavitake, A. Mehdi, L. Veyre, M. Lelli, A. Lesage, L. Emsley, C. Copéret, C. Thieuleux, J. Am. Chem. Soc. 135 (2013) 3193–3199.

[21] M.P. Conley, C. Copéret, Top. Catal. 57 (2014) 843–851.

[22] A. Quintanilla, V.C.L. Butselaar-Orthlieb, C. Kwakernaak, W.G. Sloof, M.T. Kreutzer, F. Kapteijn, J. Catal. 271 (2010) 104–114.

[23] H. Yang, S. Li, X. Zhang, X. Wang, J. Ma, J. Mater. Chem. A 2 (2014) 12060–12067.

[24] F. Wang, J. Zhao, M. Zhu, J. Yu, Y.-S. Hu, H. Liu, J. Mater. Chem. A 3 (2015) 1666–1674.

[25] J. Vignolle, T.D. Tilley, Chem. Commun. (2009) 7230–7232.

[26] S. Roland, X. Ling, M.-P. Pileni, Langmuir 32 (2016) 7683–7696.

[27] C. Xu, X. Wang, J. Zhu, J. Phys. Chem. C 112 (2008) 19841–19845.

[28] R. Ye, J. Zhao, B.B. Wickemeyer, F.D. Toste, G.A. Somorjai, Nat. Catal. 1 (2018) 318–325.

[29] M.R. Axet, O. Dechy-Cabaret, J. Durand, M. Gouygou, P. Serp, Coord. Chem. Rev. 308 (2016) 236–345.

[30] M.D. Hughes, Y.-J. Xu, P. Jenkins, P. McMorn, P. Landon, D.I. Enache, A.F. Carley, G.A. Attard, G.J. Hutchings, F. King, E.H. Stitt, P. Johnston, K. Griffin, C.J. Kiely, Nature 437 (2005) 1132–1135.

[31] M. Haruta, M. Daté, Appl. Catal. A Gen. 222 (2001) 427–437.

[32] M. Stratakis, H. Garcia, Chem. Rev. 112 (2012) 4469–4506.

[33] G.M. Veith, A.R. Lupini, S. Rashkeev, S.J. Pennycook, D.R. Mullins, V. Schwartz, C.A. Bridges, N.J. Dudney, J. Catal. 262 (2009) 92–101.

[34] H. Gu, J. Wang, Y. Ji, Z. Wang, W. Chen, G. Xue, J. Mater. Chem. A 1 (2013) 12471–12477.

[35] H. Yin, H. Tang, D. Wang, Y. Gao, Z. Tang, ACS Nano 6 (2012) 8288–8297.

[36] M. Sankar, N. Dimitratos, P.J. Miedziak, P.P. Wells, C.J. Kiely, G.J. Hutchings, Chem. Soc. Rev. 41 (2012) 8099–8139.

[37] R.J. White, R. Luque, V.L. Budarin, J.H. Clark, D.J. Macquarrie, Chem. Soc. Rev. 38 (2009) 481–494.

[38] G.G. Wildgoose, C.E. Banks, R.G. Compton, Small 2 (2006) 182–193.

[39] J. Dupont, J.D. Scholten, Chem. Soc. Rev. 39 (2010) 1780–1804.

[40] S. Sabater, J.A. Mata, E. Peris, ACS Catal. 4 (2014) 2038–2047.

[41] S. Sabater, J.A. Mata, in:, Non-Covalent Interact. Synth. Des. New Compd., John Wiley & Sons, Inc, Hoboken, NJ, 2016, pp. 313–326.

[42] S. Sabater, J.A. Mata, E. Peris, Organometallics 34 (2015) 1186–1190.

[43] D. Ventura-Espinosa, C. Vicent, M. Baya, J.A. Mata, Catal. Sci. Technol. 6 (2016) 8024–8035.

[44] D. Ventura-Espinosa, A. Marzá-Beltrán, J.A. Mata, Chem. Eur. J. 22 (2016) 17758–17766.

[45] D. Ventura-Espinosa, A. Carretero-Cerdán, M. Baya, H. García, J.A. Mata, Chem. Eur. J. 23 (2017) 10815–10821.

[46] D. Ventura-Espinosa, S. Sabater, A. Carretero-Cerdán, M. Baya, J.A. Mata, ACS Catal. 8 (2018) 2558–2566.

[47] D. Ventura-Espinosa, S. Sabater, J.A. Mata, J. Catal. 352 (2017) 498–504.

[48] L. Hintermann, A. Labonne, Synthesis 2007 (2007) 1121–1150.

[49] R. Casado, M. Contel, M. Laguna, P. Romero, S. Sanz, J. Am. Chem. Soc. 125 (2003) 11925–11935.

[50] R.E. Ebule, D. Malhotra, G.B. Hammond, B. Xu, Adv. Synth. Catal. 358 (2016) 1478–1481.

[51] D.B. Grotjahn, D.A. Lev, J. Am. Chem. Soc. 126 (2004) 12232–12233.

[52] L. Chen, C.-J. Li, Adv. Synth. Catal. 348 (2006) 1459–1484.

[53] N. Marion, R.S. Ramón, S.P. Nolan, J. Am. Chem. Soc. 131 (2009) 448–449.

[54] S. Gaillard, J. Bosson, R.S. Ramón, P. Nun, A.M.Z. Slawin, S.P. Nolan, Chem. Eur. J. 16 (2010) 13729–13740.

[55] M. Gatto, P. Belanzoni, L. Belpassi, L. Biasiolo, A. Del Zotto, F. Tarantelli, D. Zuccaccia, ACS Catal. 6 (2016) 7363–7376.

[56] P. Nun, S. Dupuy, S. Gaillard, A. Poater, L. Cavallo, S.P. Nolan, Catal. Sci. Technol. 1 (2011) 58–61.

[57] J.T. Sarmiento, S. Suárez-Pantiga, A. Olmos, T. Varea, G. Asensio, ACS Catal. 7 (2017) 7146–7155.

[58] L. Benhamou, V. César, H. Gornitzka, N. Lugan, G. Lavigne, Chem. Commun. (2009) 4720–4722.

[59] J.L. Bartels, P. Lu, A. Walker, K. Maurer, K.D. Moeller, Chem. Commun. (2009) 5573–5575.

[60] A. Mollar-Cuni, D. Ventura-Espinosa, S. Martín, Á. Mayoral, P. Borja, J.A. Mata, ACS Omega 3 (2018) 15217–15228.

[61] R. Ye, A. V. Zhukhovitskiy, R. V. Kazantsev, S.C. Fakra, B.B. Wickemeyer, F.D. Toste, G.A. Somorjai, J. Am. Chem. Soc. 140 (2018) 4144–4149.

[62] R.H. Crabtree, Chem. Rev. 112 (2012) 1536–1554.

[63] J.M. Richardson, C.W. Jones, Adv. Synth. Catal. 348 (2006) 1207–1216.

[64] N.T.S. Phan, M. Van Der Sluys, C.W. Jones, Adv. Synth. Catal. 348 (2006) 609–679.

[65] E. Bayram, J.C. Linehan, J.L. Fulton, J. a S. Roberts, N.K. Szymczak, T.D. Smurthwaite, S. Özkar, M. Balasubramanian, R.G. Finke, J. Am. Chem. Soc. 133 (2011) 18889–18902.

TOC